Iranian Journal of Materials Forming 14 (1) (2027) 23-36

IJMF

Online ISSN: 2383-0042

Iranian Journal of Materials Forming

Journal Homepage: http://ijmf.shirazu.ac.ir

Research Article

# Effect of Multidirectional Forging on Microstructure, Mechanical Properties and Corrosion Behavior of Biodegradable Zn-0.5Mg Alloy

Mohammad Javad Malekian[1], Reza Taghiabadi[1*], Mohammad Emami[2†], Morteza Saghafi Yazdi[1]

[1] Department of Metallurgy and Materials Science, Imam Khomeini International University, Qazvin, Iran
[2] Department of Materials Science and Engineering, University of Bonab, Bonab, Iran

ARTICLE INFO

*Article history:*

Received: 4 May 2026
Reviewed: 6 June 2026
Revised: 12 June 2026
Accepted: 23 June 2026

*Keywords:*

Zn-0.5Mg alloy
Biodegradable
Multidirectional forging
Mechanical properties
Corrosion behavior

*Please cite this article as:*

Malekian, M. J., Taghiabadi, R, Emami, M., & Saghafi Yazdi, M. (2027). Effect of multidirectional forging on microstructure, mechanical properties and corrosion behavior of biodegradable Zn-0.5Mg alloy. *Iranian Journal of Materials Forming*, *14*(1), 23-36. https://doi.org/10.22099/IJMF.2026.56065.1382

## ABSTRACT

The effect of multi-pass multidirectional forging (MDF) was investigated on the microstructure, mechanical properties, and corrosion behavior of the Zn-0.5Mg biodegradable alloy. According to the results, multi-pass MDF effectively modified the as-cast microstructure through the fragmentation of coarse dendrites, crushing and more uniform distribution of $Mg_2Zn_{11}$ intermetallic particles, closure of microporosities, and the formation of ultrafine grains with a crystallite size of about 10.6 nm. The yield and ultimate shear strengths of the 5-pass MDFed sample were found to be higher than those of the as-cast, 1-pass, and 3-pass MDFed samples by 42%, 26%, and 14%, and 16%, 8%, and 2%, respectively. However, following a 10% improvement in the 1-pass MDFed sample, the normal displacement of the Zn-0.5Mg alloy decreased to about 0.45 mm/mm in the 5-pass MDFed sample. The corrosion resistance of the as-cast alloy in SBF solution was improved by factors of 1.4 and 2.7 after 1 and 3 passes of MDF passes, respectively, despite the fact that alloying zinc with 0.5 wt.% Mg caused a considerable decrease in the corrosion resistance.



## 1. Introduction

Zinc is an essential element for the human body and is found in many enzymes and proteins. Sufficient amounts of Zn are required for the growth, division, and function, as well as for the metabolism of proteins and nucleic acids. On this basis, biodegradable Zn-based alloys have attracted extensive attention for biomedical applications [1, 2]. From the biodegradation point of view, Zn has a rather high chemical activity (electrode potential of -

* Corresponding author
E-mail address: taghiabadi@ikiu.ac.ir (R. Taghiabadi)

† Corresponding author
E-mail address: memami@ubonab.ac.ir (M. Emami)
https://doi.org/10.22099/IJMF.2026.56065.1382

0.762 V) which lies between that of Fe (-0.444 V) and Mg (-2.372 V) exhibiting an intermediate deterioration rate [3]. In addition, Zn exhibits excellent castability and machinability and is known as an easy-to-process material [4].

However, due to very low mechanical strength and ductility, the application of pure Zn as a potential biodegradable material is severely limited [3, 4]. Thus, considerable efforts have been made to improve the pure Zn so that it can surpass the minimum benchmarks required for biomedical applications [3]. Some of these efforts include the addition of biocompatible alloying elements, surface laser melting, chill modification, severe plastic deformation (SPD), thermomechanical processing, and related techniques.

Alloying is an effective approach for improving the overall properties of pure Zn. To date, the influence of different elements such as Li, Al, Ag, Fe, Cu, Mn, Ca, Sr, Bi, Zr, and Ti has been examined with respect to the mechanical properties and corrosion behavior of pure Zn [3, 5]. Magnesium is an alloying element that has received considerable attention. It is non-toxic, and due to its very low solid solubility in Zn, its addition causes the formation of the hard $Mg_2Zn_{11}$ compound in the matrix increasing the alloy's hardness and strength. The gradual degradation of Mg in the body environment may encourage cell proliferation and bone regeneration. Moreover, the concurrent release of $Zn^{2+}$ and $Mg^{2+}$ not only increases the alloy's biocompatibility, but also enhances its corrosion rate [5, 6].

However, due to the precipitation of a high fraction of brittle $Mg_2Zn_{11}$ intermetallics, the excessive addition of Mg drastically lowers the ductility and toughness of Zn–Mg alloys unfavorably affects their corrosion resistance [7]. Accordingly, in recent years, researchers have focused their attention on developing dilute Zn-Mg alloys (≤1 wt.% Mg) for the manufacture of biomedical devices such as cardiovascular stents, orthopedic implants, and wound-closure materials [7-10]. Decreasing the Mg content, however, also reduces the mechanical properties of the alloys, necessitating minor addition of other alloying elements such as Sr, Mn, Cu, and Ca [6, 11], the addition of reinforcing particles [12] and/or the implementation of supplementary processes such as thermomechanical processing and severe plastic deformation (SPD) [13].

Multidirectional forging is one of the well-known SPD processes that can be implemented on an industrial scale. This method has been considered an appropriate approach for the structural modification and properties enhancement of HCP alloys such as Zn [14]. The simple geometry of the forging die, low implementation cost, high efficiency, and high repeatability distinguish MDF among other SPD processes. In this process, a rectangular block is exposed to forging in different directions without altering its horizontal dimensions. In each deformation cycle, the block is rotated by 90 degrees about its central axis to achieve a more uniform microstructure by changing the loading sequence. This process causes the grain size to decrease, resulting in a final microstructure with finer grains than the initial state. The grain refinement begins in the central part of the sample, but as the number of passes increases, a more uniform microstructure is formed throughout the central region [14, 15].

Various research studies have reported the positive influence of MDF on the microstructure refinement and homogenization of the as-cast Zn-based alloys and composites such as Zn–24Al–2Cu [16], ZA27–SiC [17], ZA22/SiP [18, 19], Zn–Al–Cu–Mg [20], and Zn-Si alloys [21]. However, to the best of our knowledge, no study has investigated the effect of MDF on the microstructure, mechanical properties, and corrosion behavior of Zn-0.5Mg alloy. Building on this foundation, the MDF technique was selected to investigate its efficacy in refining and homogenizing the microstructure, as well as enhancing the mechanical and corrosion behavior of the Zn-0.5Mg alloy.

## 2. Experimental Procedure

The experimental Zn–0.5Mg alloy was prepared in a resistance furnace (3-phase AZAR-VM2L-1200, 2.2 kW) employing a silicon carbide crucible. For this purpose, primary Zn ingots (99.9 wt. %) were melted under a $ZnCl_2$-based flux cover. Then, the desired amount of preheated Mg (99.9 wt.%) was added to the melt. The melt was subsequently heated up to about 870 °C, stirred gently, and poured into a cast iron mold. The average solidification cooling rate of the mold was determined to be about 4.2 °C/s. The chemical analysis of the prepared alloy is shown in Table 1.

The MDF samples, measuring 15×10×10 $mm^3$ (Fig. 1(a)), were extracted from the castings by wire-cut machine. The MDF die (Fig. 1(b-1) and 1(b-2)) was made of hardened and tempered (50±2 HRC) H13 hot-work tool steel with a central cavity measuring 40×15×10 $mm^3$. The details of the die are presented in [22]. The MDF operation was performed at room temperature using a 100 -ton hydraulic press at a ram speed of 1.6 mm/s. The MDF process was conducted for one, three, and five passes and the sample was rotated by 90° about the x- and y-axis, respectively after each pass (Fig. 2). The strain applied in each MDF pass, calculated using the following equation, was determined to be about 0.47:

$$\varepsilon = \frac{2}{\sqrt{3}} \ln \frac{H}{W} \tag{1}$$

Where *H* and *W* are the height and width of the sample, respectively [22].

**Table 1.** Chemical composition of pure Zn and Zn-0.5Mg alloy (wt.%)

| Zn | Sample code | Mg | Pb | Cd | Cu | Sn | Other | Rem. |
|---|---|---|---|---|---|---|---|---|
| Zn-0.5Mg | M5 | 0.54 | 0.005 | 0.001 | 0.002 | 0.005 | < 0.01 | Zn |

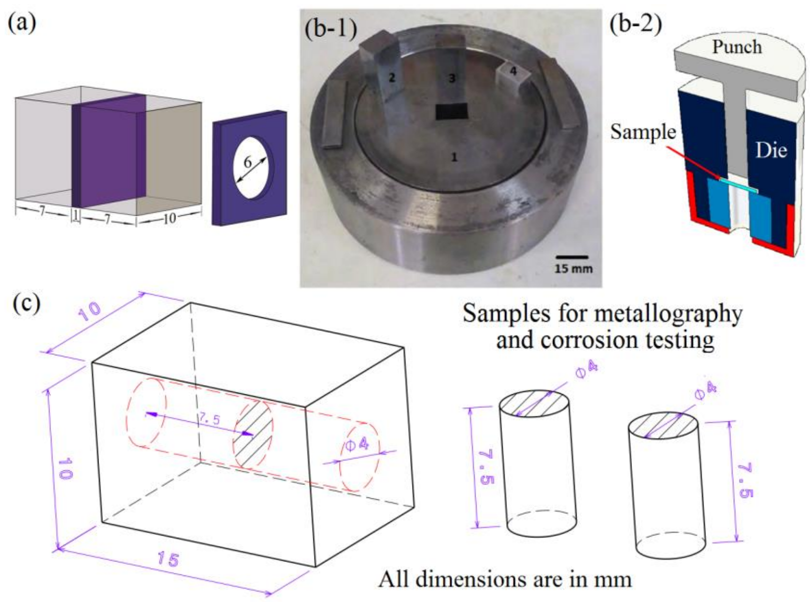


**Fig. 1.** (a) Sampling location of shear punching specimens in MDF-processed sample, (b-1) the MDF die, (b-2) schematic of shear punching process, and (c) sampling location and geometry of corrosion testing and metallography specimens.

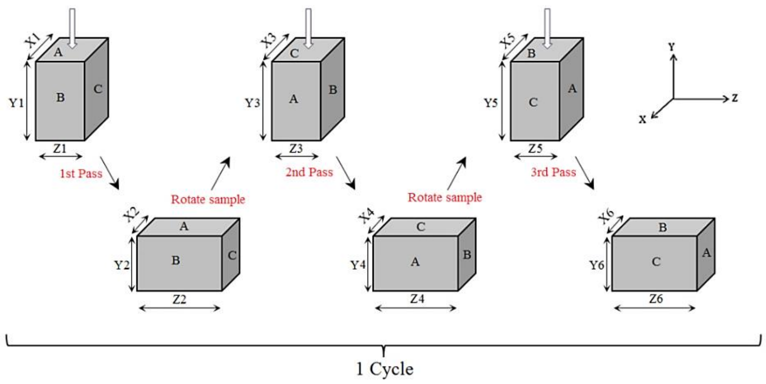


**Fig. 2.** Schematic illustration of the MDF process and the sequence of sample processing.

The room temperature Vickers microhardness of the MDF-processed samples was determined on their cross-sections using a KOOPA tester (model UV1) in accordance with ASTM E-92. Shear punch testing was performed to measure the mechanical properties of the samples. The schematic diagrams showing the sampling location for shear punch testing and the shear-punching die are shown in Fig. 1(a) and 1(b), respectively. The shear punch tests were conducted by using a Zwick/Roell-*Z100* universal testing machine at a constant crosshead speed of 0.001 mm/s. The shear stress (τ, MPa) and normal displacement (x, mm/mm) values were calculated using Eqs. (2) and (3), respectively [23]. In these equations, *P* is the applied force, *t* represents the thickness of the sample, and *d* is the average punch/die diameter in (mm):

$$\tau = \frac{P}{\pi dt} \tag{2}$$

$$x = \frac{h}{t} \tag{3}$$

The metallography surfaces were prepared by mechanical grinding using SiC paper (P320 to P3000) followed by mechanical polishing using a 1 µm diamond paste. It is worth noting that the metallographic samples were taken from the central region of the MDF-processed samples to achieve maximum microstructural uniformity (Fig. 1(c)). The samples were etched using a 3 vol.% Nital solution (3 ml $HNO_3$ + 97 ml Ethanol) to reveal the microstructure. The microstructure was then characterized using an Olympus BX60 optical microscope (OM) and a VEGA TESCAN-LMU scanning electron microscope (SEM) equipped with energy-dispersive X-ray spectroscopy (EDS). An X-ray diffraction (XRD) diffractometer (Philips Expert Pro, 45 kV voltage) was utilized to identify the existing phases and crystallite size using Cu-Kα radiation with a wavelength of $\lambda = 1.56$ Å over the 2θ=20-80°. Digimizer software (5.4.9) was also used to analyze the metallographic images.

To evaluate the porosity content, the density of all samples was measured by the Archimedes' immersion method. For this purpose, the samples weights were determined in air ($m_a$) and in water ($m_w$) using a BP210S Balance (Sartorius AG, *Göttingen*, Germany). The experimental density ($\rho_r$) was then calculated using Eq. (4):

$$\rho_r = \frac{m_a}{m_a - m_w} \tag{4}$$

The porosity content was calculated using Eq. (5):

$$\%P = \frac{\rho_{th} - \rho_r}{\rho_{th}} \tag{5}$$

Where, $\rho_r$ and $\rho_{th}$ are the experimental and theoretical densities of the sample, respectively [24].

To evaluate the corrosion behavior of the materials, potentiodynamic polarization experiments were performed on pure zinc, as-cast, and MDF-processed Zn-0.5Mg samples (Fig. 1(c)) in simulated body fluid (SBF) using a 3-electrode set-up comprising a tungsten electrode, a saturated calomel electrode, and the test specimen as the counter, reference, and working electrodes, respectively.

## 3. Results and Discussion

### *3.1. Effect of multi pass MDF on the microstructure of Zn-0.5Mg alloy*

Fig. 3(a)-3(c) depicts the as-cast microstructure of the Zn-0.5Mg alloy. As can be seen, the main microstructural constituents of the alloy are bright dendrites and dark interdendritic regions, which according to the EDS analysis, contain considerable amounts of Mg (Fig. 3(d)). To clarify the alloy micro-constituents, the solidification process of the alloy was analyzed using the Zn-Mg binary phase diagram (Fig. 4). According to the phase diagram, the solidification of the alloy starts at about 410 °C with the formation and growth of α-Zn dendrites in L+α-Zn mushy zone. Due to the segregation of Mg atoms into the remaining liquid, the Mg concentration in the interdendritic region increases up to approximately 2.72 wt.% Mg [21] at about 367.2 °C, where the liquid is transforms into a eutectic mixture comprising α-Zn + $Mg_2Zn_{11}$.

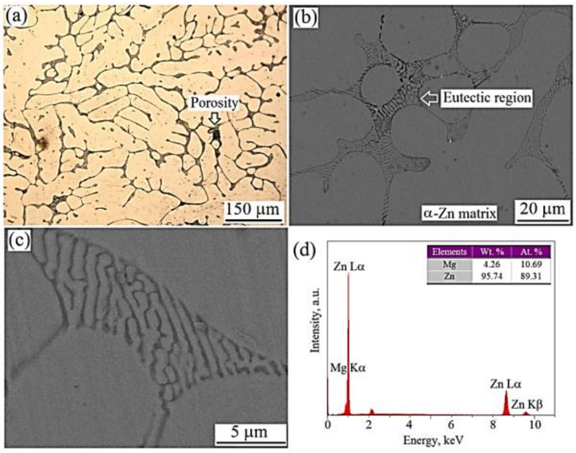


| Elements | Wt. % | At. % |
|---|---|---|
| Mg | 4.26 | 10.69 |
| Zn | 95.74 | 89.31 |

**Fig. 3.** As-cast microstructure of Zn-0.5Mg alloy observed by (a) OM and (b) SEM, (c) enlarged view of the eutectic region in micrograph (b), (d) SEM-EDS analysis of the eutectic region.

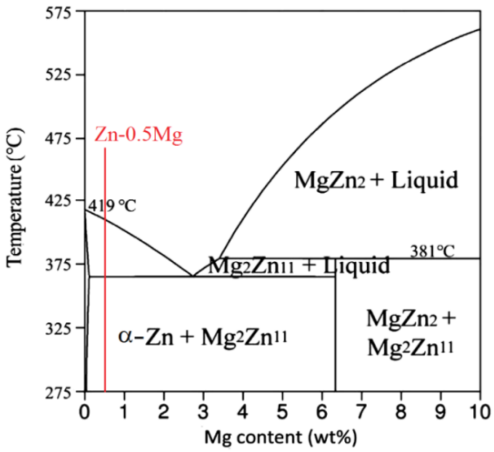


**Fig. 4.** Zn-Mg phase diagram [21].

According to the solidification analysis, it seems that the bright regions in the alloy microstructure are the α-Zn dendritic network, whilst the black interdendritic regions are two-phase layered structure comprising α-Zn and $Mg_2Zn_{11}$. According to the image analysis results, the area fraction of the eutectic component was about 13.20±2.59%. In agreement with these observations, the XRD analysis (Fig. 5(a)) also shows the presence of the $Mg_2Zn_{11}$ compound within the α-Zn matrix. It is also evident from the XRD analysis that applying multi-pass MDF did not result in any specific phase transformation in the alloy.

The effect of multi-pass MDF on the Zn-0.5Mg alloy microstructure is depicted in Fig 6. As shown, applying MDF considerably deforms the as-cast microstructure, which manifests itself as plastic flow lines and, accordingly, the gradual elimination of the coarse primary dendrites, crushing of the $Mg_2Zn_{11}$ intermetallics into smaller particles, forging porosities and forming a dense, homogeneous and well-refined microstructure. Furthermore, due to the increased cumulative strain, increasing the number of MDF passes causes more microstructural modification, and promotes a more homogenized structure (Fig. 6(b)-6(d)).

Considering the restricted number of available slip systems in HCP-structured Zn alloys, their plastic deformation is essentially accommodated through twinning rather than basal dislocation slip [25, 26]. Nevertheless, the twining mechanism is not capable of producing extensive plastic deformation. Indeed, the importance of MDF-twinning lies in its ability to rearrange slip systems into appropriate orientations relative to the loading direction, thereby facilitating further slip and plastic deformation [27]. Some research works have also been conducted on the effect of MDF on the microstructure of Zn-based alloys [12, 28-33], most of which emphasize its positive impact on the refinement and uniform distribution of second phase particles. However, the work con ducted by Mollaei et al. [28] revealed that applying multi-pass MDF, although it refines the $Mg_2Zn_{11}$ particles, cannot improve their distribution within the matrix of as-extruded Zn-0.2Mg alloy.

Multi-pass MDF also encourages the formation of an ultrafine grained structure. It is worthwhile to note that, as a result of its high crystallographic anisotropy, the as-cast grain structure of pure Zn consists of coarse columnar grains (3216±1043 μm) associated with

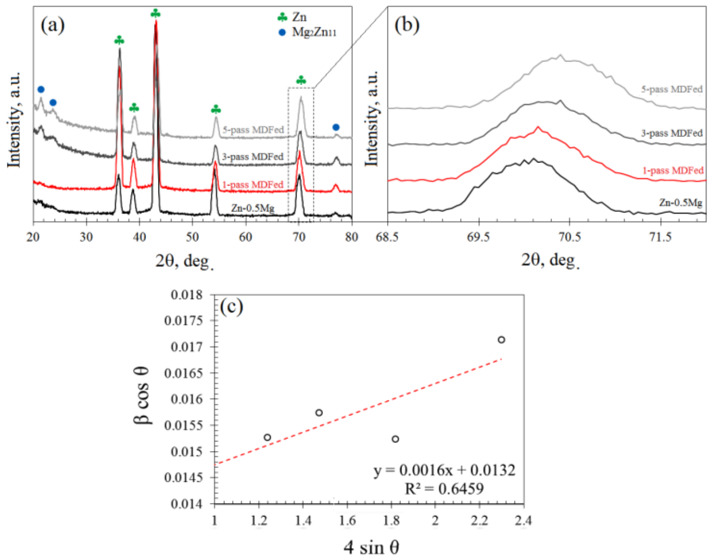


**Fig. 5.** (a) XRD patterns of the as-cast and multi-pass MDFed samples, (b) locally-enlarged view of the marked region in 5(a) showing peaks broadening and shifting, and (c) Williamson-Hall plot for the 5-pass MDFed sample to estimate the sample's crystallite size after MDF.

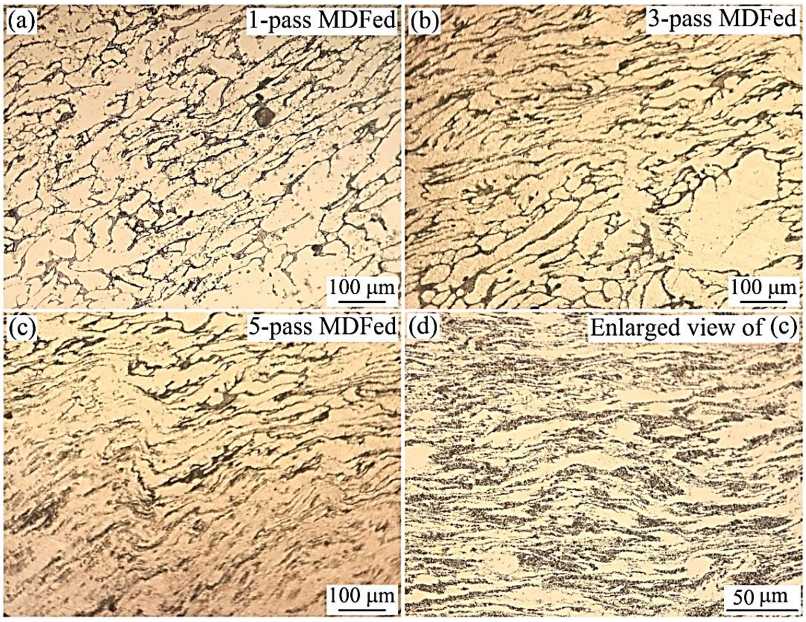


**Fig. 6.** OM micrographs showing the microstructure of the Zn-0.5Mg alloy after (a) 1-pass MDF, (b) 3-pass MDF, (c) 5-pass MDF, and (d) a higher magnification view of micrograph (c).

$[1\bar{1}01]/(1\bar{1}02)$ twins [21]. The addition of Mg, due to its very low equilibrium partition coefficient in Zn ($k_0$ = 0.05) causes a considerable growth restriction effect (constitutional undercooling), promoting the formation of fine equiaxed grains. Moreover, there are reports demonstrating the high potential of HCP-structured $MgZn_2$ particles for the heterogeneous nucleation of α-Zn grains in Zn-Mg alloys containing less than 6.3wt. %, which is attributed to the non-equilibrium solidification and/or Mg concentration inhomogeneity in the molten alloy [34].

Applying MDF further refines the primary α-Zn grains, which can be described by the occurrence of dynamic recrystallization (DRX) [31]. Room-temperature formation of DRXed grains has been previously reported in SPD processed Zn-based alloys [35] and was ascribed to the low melting temperature/low stacking fault energy (SFE) of Zn. Particle stimulated nucleation (PSN) is thought to be another mechanism involved in the formation of the fine-grained structure in MDFed alloys. This mechanism generally occurs in alloys with high fractions of rather coarse second-phase particles larger than 1 μm in size [36]. Due to plastic deformation incompatibility with the matrix, the $Mg_2Zn_{11}$ particles are likely to act as effective barriers to the motion of dislocations generating high dislocation pile-ups and highly strained fields (HSFs) at their interfaces [36], thereby activating a large number of slip systems and promoting DRX. According to Ref. [37], the HSFs can act as favorable sites for the nucleation of DRXed grains. The highly-fractured $Mg_2Zn_{11}$ particles may also hinder the growth of DRXed grains via the Zener pinning mechanism. In Zener pinning, the interaction of grain boundaries with second phase particles reduces their energy via reducing their area. Therefore, the ultrafine $Mg_2Zn_{11}$ particles in the microstructure of the MDFed samples are likely to serve as potent sites for Zener pinning.

The Williamson-Hall plot of the main α-Zn peaks (2θ = 36.1°, 43.2°, 54.1°, and 70.2°) (Fig. 3(d)) also reveals that the average crystallite size is reduced to about 10.6 nm demonstrating the MDF potential in producing a fine-grained microstructure. The positive impact of MDF on the grain size of Zn-based alloys has been previously demonstrated elsewhere. Neres da Silva et al. [33] showed that applying room temperature MDF causes substantial refinement of the Zn-3.8Al-2.3Cu-0.4Mg alloy grain size from 53±10 μm in the as-cast state to approximately 33±12 μm, 32±10 μm, 2.1±1 μm, 0.3±0.1 μm, and 0.25±0.1 μm in the 1-, 2-, 4-, 8-, and 23 passes MDFed samples, respectively. Liu et al. reported that six passes of MDF at 200 °C can refine the initial grains of the Zn-1.5Mg alloy (~ 200 μm) by 96%. Also, Mollaei et al [28] performed three passes of warm (100 °C) MDF on the as-extruded Zn-0.2Mg alloy and achieved grain refinement from about 17.2±0.5 μm to 1.9±0.3 μm. He et al [32] also reported that the average grain size of as-extruded Zn-0.2Mg alloy (~ 10.4 μm) decreased to 3.7, 3.4, and 3.2 μm following 6, 12, and 18 MDF passes, respectively. This refinement was attributed to the occurrence of DRX. The area fraction of DRXed grains also increased from 14.09% after 6 passes of MDF to 71.40% at 12 passes, whilst it decreased to 62.54% after 18 passes.

### *3.2. Effect of multi pass MDF on the mechanical properties of the Zn-0.5Mg alloy*

Fig. 7(a) depicts the variation of shear strength as a function of normal displacement for the experimental samples. The effect of the MDF pass number on the yield shear strength (YSS) and ultimate shear strength (USS) of the experimental samples is also presented in Fig. 7(b). As shown, applying multi-pass MDF progressively enhances both the YSS and USS, whilst reducing the ductility (Fig. 7(a)).

According to Fig. 7(b), the YSS and USS of the 5-pass MDFed sample are higher than those of the as-cast, 1-pass, and 3-pass MDFed samples by 42, 26, and 14%, respectively, and by 16%, 8%, and 2%, respectively. Moreover, the normal displacement of the 5-pass MDFed sample is lower than that of the as-cast, 1-pass, and 3-pass MDFed samples by about 14%, 22%, and 15%, respectively. It can be also seen that the YSS and USS values become gradually closer to each other probably due to microstructural homogenization and the formation of the ultrafine grains. The effect of multi- pass MDF on the macro- and micro-hardness, and the porosity content of the experimental alloys is also illustrated in Fig. 8.

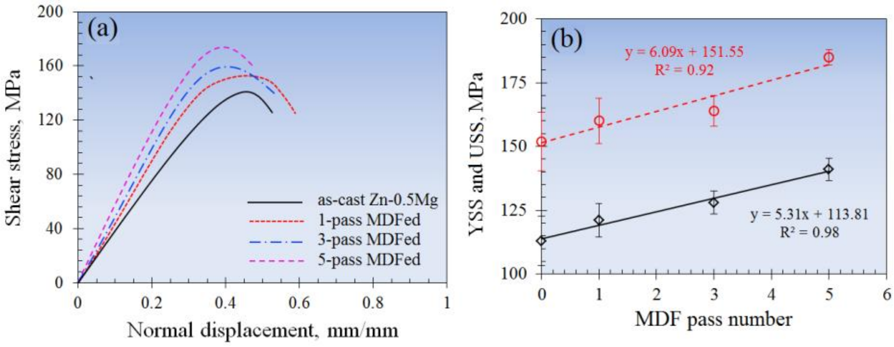


**Fig. 7.** Variation of shear stress as a function of normal displacement for the as-cast and multi-pass MDFed Zn-0.5Mg alloys.

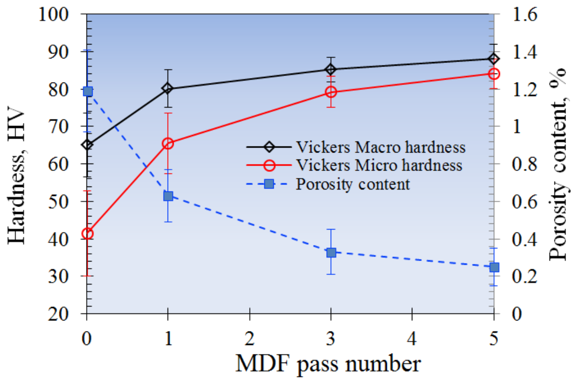


**Fig. 8.** Effect of multi-pass MDF on the Vickers macro- and micro-hardness, and the porosity content of the experimental alloys.

These results are in agreement with previous findings. According to He et al. [32], applying MDF increases the initial microhardness of the as-extruded Zn-0.2Mg alloy from about 91 HV to about 102 HV and 107 HV following 6 and 12 cycles, respectively, whilst it slightly declined to about 101 HV at 18 MDF cycles. They also showed that the UTS of as-extruded Zn-0.2Mg alloy increased from approximately 309 MPa of the as-extruded condition to 397, 408, and 408 MPa following 6, 12, and 18 MDF cycles, respectively. In line with our results, they showed a decline in elongation from about 28% in the as-extruded state to about 22% and 19% following 6 and 18 MDF cycles, respectively.

Considering the microstructural characterization results (Figs. 4 and 6), the mechanical strength improvement of the Zn-0.5Mg alloy following the multi-pass MDF can be explained by the concurrent influence of various process-related mechanisms, namely, crushing of the dendritic network, refinement and uniform distribution of hard $Mg_2Zn_{11}$ intermetallics, which promote PSN and Orowan strengthening, grain refinement of the as-cast Zn-0.5Mg alloy (Fig. 5(c)) (grain boundary strengthening), an increase in the density of geometrically necessary dislocations (GNDs) (dislocation strengthening), and microstructural densification through the reduction of porosity (Fig. 8). It is worth noting that, porosities act as stress concentration sites within the microstructure, impairing the shear properties by promoting the initiation and propagation of microcracks.

Due to the brittle nature of the $Mg_2Zn_{11}$ compound [31], the presence of a continuous α-Zn/$Mg_2Zn_{11}$ eutectic interdendritic network in the as-cast Zn-0.5Mg alloy negatively affects its mechanical properties through facilitating the initiation and propagation of microcracks. However, the crushing and uniform distribution of the $Mg_2Zn_{11}$ particles increase their number density enhancing their load-bearing potential and reducing the stress concentration developed around each particle, while increasing their Zener pinning efficiency against grain boundary motion. The severe shearing of the material during the MDF is also likely to promote intimate contact between the $Mg_2Zn_{11}$ particles and the α-Zn matrix improving their load-transfer characteristics [31] thereby decreasing the chance of crack nucleation and growth contributing to the alloy strengthening (load-transfer strengthening). Orowan strengthening by well-refined $Mg_2Zn_{11}$ particles can also participate in the strength improvement of Zn-0.5Mg alloy via restricting the movement of dislocation and promoting the formation of dislocation loops.

The Hall-Petch and dislocation strengthening mechanisms are also thought to be involved in the overall strengthening of the MDFed alloys. The Hall-Petch strengthening mechanism is governed by the substitution of coarse initial grains with ultrafine dynamically-recrystallized grains. The dislocation strengthening mechanism also appears to be activated by the generation of GNDs at the matrix/ $Mg_2Zn_{11}$ particles interface. Due to the different elastic moduli of the matrix and intermetallic particles (i.e., their high strain-incompatibility), the formation of GNDs in the course of shear loading is thought to occur as a result of development of intensive strain gradients adjacent to the hard $Mg_2Zn_{11}$ particles. This in turn increases the fraction of high-angle grain boundaries (HAGBs) which contribute to alloy strengthening by impeding the gliding of dislocations [28, 36, 38].

The pile-up of GNDs (i.e., strain concentration) at the vicinity of $Mg_2Zn_{11}$ particles may promote interfacial micro-voids which can coalesce and form microcracks impairing the alloy ductility [36]. It is noted that, as an intermetallic compound, $Mg_2Zn_{11}$ due to its high melting entropy ($\Delta S/R \approx \alpha > 2$) [39] provide a large Jackson's coefficient and a faceted-type interface at the atomic scale favoring the nucleation of micro-voids/microcracks increasing the chance of particle-matrix decohesion. Micro-porosities also serve as stress-concentrators within the matrix facilitating the nucleation and propagation of microcracks impairing the alloy strength/ductility. Therefore, their forging and/or dispersion throughout the matrix can improve the alloy hardness and shear properties.

### *3.3. Effect of multi pass MDF on the corrosion properties of the Zn-0.5Mg alloy*

The potentiodynamic polarization curves of pure zinc, the as-cast Zn-0.5Mg, and the Zn-0.5Mg MDFed for 1 and 3 passes in 3.5 wt.% NaCl solution can be seen in Fig. 9. The polarization parameters obtained from the Tafel extrapolation method are summarized in Table 2. According to Fig. 9, nearly all specimens show rapid anodic dissolution with no passive region. It is evident that the corrosion current density ($i_{corr}$) increased from 62.4 μA/cm$^2$ in pure zinc to 169 μA/cm$^2$ in the as-cast Zn-0.5Mg, which indicates a 2.7-fold increase in the corrosion rate of the as-cast alloy. An increased corrosion rate of pure zinc with the addition of small amounts of Mg has been reported by Wang et al. [40] in their study of Zn-Mg alloys in a $Ca(OH)_2$ solution. The higher corrosion rate of the as-cast Zn-0.5Mg alloy may be attributed to galvanic coupling between the substrate and the $Mg_2Zn_{11}$ phase. Employing 1 and 3 MDF passes resulted in 1.4 and 2.7-fold decreases, respectively, in the corrosion current density of the Zn-0.5Mg alloy, indicating a significant improvement in the corrosion resistance of the Zn-0.5Mg alloy with the MDF passes. Regarding the corrosion potential, the addition of 0.5 wt.% Mg to pure zinc caused a slight shift in the corrosion potential toward more noble potentials. The reason for this behavior is not yet fully understood.

The SEM micrographs of the corroded surface of the as-cast, and 1-pass, and 3-pass MDFed Zn-0.5Mg alloys are presented in Fig. 10. The surface of the as-cast specimen (Fig. 10(a)) shows a severe corrosion with indications of localized corrosion. Higher magnification images in Fig. 10(b) and 10(c) show the formation of grooves, possibly as a result of the preferential attack on the eutectically solidified region and the dissolution of local anodes. The surface morphology of the corroded 1-pass specimen in Figs. 10(e) and 10(f), shows smaller corroded areas that are distributed throughout the surface, suggesting higher corrosion resistance compared to the as-cast sample. Consistent with the polarization results, the 3-pass MDFed sample, with the smallest size of the corroded areas associated with the eutectic regions, was the least severely corroded Zn-0.5Mg alloy. According to the SEM observations, the matrix α-Zn showed no significant corrosion attack and the polishing scratches were still evident.

Having a homogeneous single-phase microstructure without any intermetallic second phases, pure zinc is expected to show higher corrosion resistance than the Zn-0.5Mg alloy. According to Fig. 3, the microstructure of the Zn-0.5Mg alloy consists of α-Zn matrix and a eutectic mixture of α+$Mg_2Zn_{11}$. This microstructural inhomogeneity promotes micro-galvanic corrosion. This can explain the higher corrosion rate of the Zn-0.5Mg alloy compared to that of pure zinc. Zn-Mg intermetallics are reportedly more active than pure Zn in the galvanic series [19, 40, 41]. Thus, in a galvanic couple of Zn and $Zn_2Mg_{11}$, the $Zn_2Mg_{11}$ intermetallic phase dissolves preferentially, probably due to the following reaction.

$$Zn_{11}Mg_2 \rightarrow 2Mg^{2+} + 11Zn^{2+} + 26e^- \quad (6)$$

The following reactions may be proposed for the

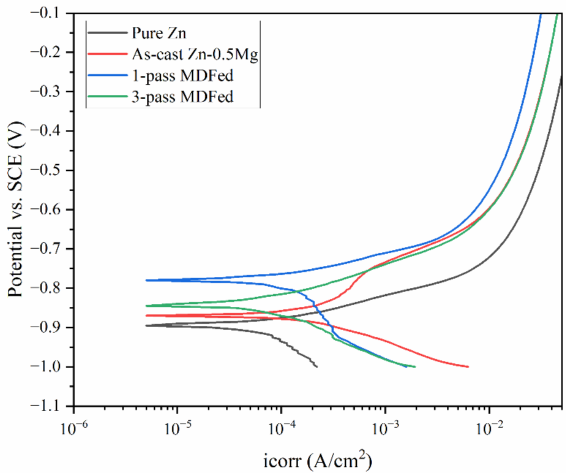


**Fig. 9.** Potentiodynamic polarization curves of the different alloys corroded in 3.5 wt.% NaCl solution.

**Table 2.** Polarization parameters for the different specimens in 3.5 wt.% NaCl solution

| | $E_{corr}$ (V) | $i_{corr}$ ($\mu A/cm^2$) | $\beta_a$ (mV/dec) | $\beta_c$ (mV/dec) |
|---|---|---|---|---|
| Pure Zn | -0.9 | 62.4 | 60 | 160 |
| Zn-0.5Mg (base) | -0.87 | 169 | 150 | 80 |
| Zn-0.5Mg (1-pass) | -0.77 | 122 | 90 | 329 |
| Zn-0.5Mg (3-pass) | -0.84 | 62 | 80 | 110 |

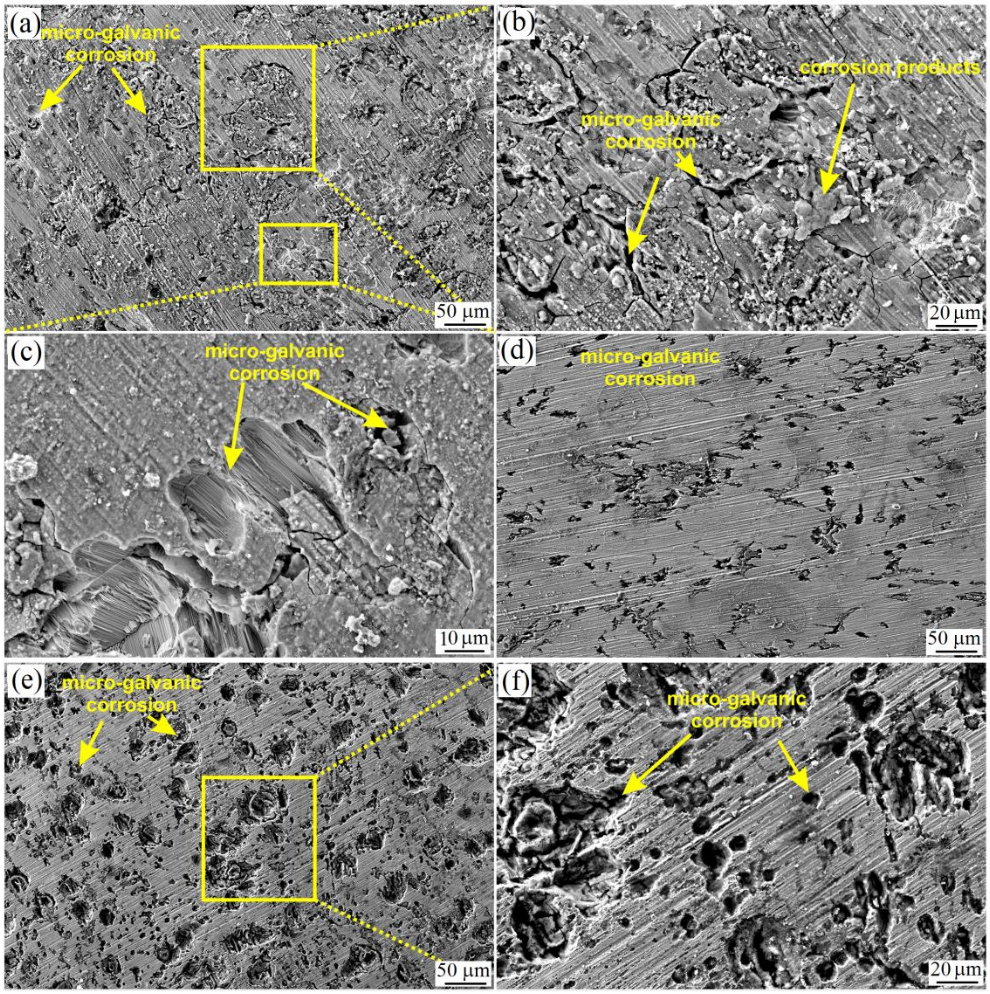


**Fig. 10.** SEM micrographs of the surface of the Zn-0.5Mg alloys corroded in Ringer's solution. (a, b, c) as-cast alloy; (d) 3-pass MDFed alloy, (e, f) 1-pass MDFed alloy.

cathodic reaction and the formation of zinc and Mg hydroxides:

$$2H_2O + O_2 + 4e^- \rightarrow 4OH^- \quad (7)$$

$$Zn^{2+} + 2OH^- \rightarrow Zn(OH)_2 \quad (8)$$

$$Mg^{2+} + 2OH^- \rightarrow Mg(OH)_2 \quad (9)$$

The formation of Mg oxide/hydroxide films on Zn-Mg alloys may partially protect the alloy surface from corrosion.

Previous studies have shown that both the Mg content and the microstructure of a Zn-Mg alloy can affect the alloy's corrosion resistance [41]. However, it has been argued that in low Mg contents like 0.5 wt.%, microstructure plays a more vital role in the corrosion behavior of Zn-Mg alloys than the composition itself [42].

According to the literature [41, 43] and based on the SEM observations (Fig. 10), the corrosion attack initiates at the eutectic regions. In these regions, small anodes ($Mg_2Zn_{11}$) and cathodes ($\alpha$-Zn lamellae) can act as potential corrosion initiation sites via microgalvanic corrosion. MDF processing leads to a more refined microstructure of both the primary α-Zn and the eutectic mixture. A more refined microstructure with regard to the size of the intermetallic phase and/or the interlamellar eutectic spacing can lead to an improved corrosion resistance of the alloy [41, 44-46]. The eutectic mixtures are expected to drive localized microgalvanic corrosion. A finer microstructure means a closer distance between the fine anodic and cathodic regions. In a refined microstructure, the number of grain boundaries as the fast diffusion paths increases, which in turn leads to a faster formation of passive films on the alloy surface. Thus, a more homogeneous distribution of the local anodes and cathodes, together with their smaller size resulting from an increasing number of MDF passes, gives rise to a more homogenous and less severe corrosion attack. These results are in accordance with the study of Ye et al. [47] on Zn-Mg binary alloys in SBF solution.

Other factors that may affect the alloy's corrosion behavior are the development of internal stresses and crystal imperfections due to the MDF process. A slight shift in the peak positions towards higher angles in the MDFed samples (Fig. 5(b)) may be associated with the accumulation of compressive lattice microstrains. The broadening of diffraction peaks (Fig. 5(b)) can also indicate an increase in the dislocation density [48]. These changes may enhance the alloy's surface energy and accelerate the reaction rate with the corrosive media, assisting the rapid formation of the corrosion products on the surface and the later possible protective role [12]. However, it seems that the role of microstructure in the present study is more significant as discussed earlier.

## 4. Conclusions

1- The Zn-0.5Mg alloy microstructure consists of an α-Zn dendritic network and a layered eutectic structure comprising α-Zn and $Mg_2Zn_{11}$. The area fraction of the eutectic component was about 13.20±2.59%.

2- Applying MDF considerably deforms the as-cast microstructure which manifests itself as plastic flow lines and, accordingly, the gradual elimination of the coarse primary dendrites, crushing of the $Mg_2Zn_{11}$ intermetallics into smaller particles, closure of porosity and the formation of a dense, homogeneous and well-refined microstructure. According to the XRD analysis, the crystallite size of the 5-pass MDFed sample was estimated to be approximately 10.6 nm.

3- The yield and ultimate shear strengths of the 5-pass MDFed sample were higher than those of the as-cast, 1-pass, and 3-pass MDFed samples by 42%, 26%, and 14%, respectively**,** and by 16%, 8%, and 2%, respectively. Moreover, the normal displacement of 5-pass MDFed sample was lower than that of the as-cast, 1-pass, and 3-pass MDFed samples by about 14%, 22%, and 15%, respectively.

4- -The potentiodynamic polarization results showed that 1 and 3 MDF passes resulted in a significant improvement in the corrosion resistance of the as-cast Zn-0.5Mg alloy. This was attributed to the more refined and better distributed interlamellar spacing in the eutectically solidified regions, which act as corrosion initiation sites.

## Authors' contributions

**M. J. Malekian:** Conceptualization, Methodology, Resources, Investigation, Software, Writing - original draft

**R. Taghiabadi**: Project administration, Methodology, Supervision, Writing - review & editing

**M. Emami:** Project administration, Methodology, Supervision, Writing - review & editing, Visualization

**M. Saghafi Yazdi:** Project administration, Methodology, Supervision

## Conflict of interest

The author declares that there is no conflict of interest regarding in this research.

## Funding

This research has not received any funding.

## Data availability

The raw data can be obtained on request from the corresponding author.

## 5. References


[1] Shishir, R., Nasiruddin, U., Manojkumar, P., Lokeshkumar, E., Ponnilavan, V., Parfenov, E. V., Valiev, R. Z., & Rameshbabu, N. (2023). Zinc as a potential bio-degradable temporary implant material. *Materials Today: Proceedings*. https://doi.org/10.1016/j.matpr.2023.09.009

[2] Sułkowski, B., Pałka, P., Boczkal, G., Lee, R., Horky, J., Zehetbauer, M. J., & Schafler, E. (2025). Mechanical and corrosion properties of Zn-0.5 Mg and Zn-1.0 Mg alloys processed by HPT. *Materials Science and Engineering: A, 930*, 148139. https://doi.org/10.1016/j.msea.2025.148139

[3] Kabir, H., Munir, K., Wen, C., & Li, Y. (2021). Recent research and progress of biodegradable zinc alloys and composites for biomedical applications: Biomechanical and biocorrosion perspectives. *Bioactive Materials,* 6(3), 836-879. https://doi.org/10.1016/j.bioactmat.2020.09.013

[4] Akbari, F., Golkaram, M., Beyrami, S., Shirazi, G., Mantashloo, K., Taghiabadi, R., Yazdi, M. S., & Ansarian, I. (2024). Effect of solidification cooling rate on microstructure and tribology characteristics of Zn-4Si alloy. *International Journal of Minerals, Metallurgy and Materials, 31*(2), 362-373. https://doi.org/10.1007/s12613-023-2764-9

[5] Mostaed, E., Sikora-Jasinska, M., Drelich, J. W., & Vedani, M. (2018). Zinc-based alloys for degradable vascular stent applications. *Acta Biomaterialia, 71*, 1-23. https://doi.org/10.1016/j.actbio.2018.03.005

[6] Ji, C., Ma, A., Jiang, J., Song, D., Liu, H., & Guo, S. (2024). Research status and future prospects of biodegradable Zn-Mg alloys. *Journal of Alloys and Compounds, 993,* 174669. https://doi.org/10.1016/j.jallcom.2024.174669

[7] Milenin, A., Kustra, P., Lelek-Borkowska, U., Wróbel, M., Marzec, M., Sulej-Chojnacka, J., Półrolniczak, J., Polkowska, I., & Nowicka, B. (2024). In vitro and in vivo degradation of the new dissolvable surgical wire, produced from Zn based low alloy by hot and cold drawing. *Metallurgical and Materials Transactions A, 55*(9), 3434-3449. https://doi.org/10.1007/s11661-024-07470-0

[8] Jin, H., Zhao, S., Guillory, R., Bowen, P. K., Yin, Z., Griebel, A., Schaffer, J., Earley, E. J., Goldman, J., & Drelich, J. W. (2018). Novel high-strength, low-alloys Zn-Mg (<0.1wt% Mg) and their arterial biodegradation. *Materials Science and Engineering: C,* 84, 67-79. https://doi.org/10.1016/j.msec.2017.11.021

[9] Li, R., Ding, Y., & Zhang, H. (2023). Toughness and strength coordination in a low-alloy Zn–0.5 Mg alloy via extrusion and post-deformation annealing. *Metals and Materials International, 29*(10), 2807-2825. https://doi.org/10.1007/s12540-023-01420-y

[10] Pieła, K., Błaż, L., Bochniak, W., Ostachowski, P., Łagoda, M., Żabiński, P., Jaskowski, M., Kiper, M., & Polkowska, A. (2019). Self-hardening of low-alloyed zinc for biodegradable application. *Journal of Alloys and Compounds, 810*, 151883. https://doi.org/10.1016/j.jallcom.2019.151883

[11] Voshage, M., Megahed, S., Schückler, P. G., Wen, P., Qin, Y., Jauer, L., Poprawe, R., & Schleifenbaum, J. H. (2022). Additive manufacturing of biodegradable Zn-xMg alloys: Effect of Mg content on manufacturability, microstructure and mechanical properties. *Materials Today Communications, 32,* 103805. https://doi.org/10.1016/j.mtcomm.2022.103805

[12] Hashemizarandi, S., Riazat, A., Emami, M., & Taghiabadi, R. (2025). Effect of multi-pass multidirectional forging on microstructure and corrosion behavior of Zn-1Fe biodegradable alloy. *Journal of Alloys and Compounds, 1038*, 182810. https://doi.org/10.1016/j.jallcom.2025.182810

[13] Ge, G., He, X., Guo, Y., Yang, G., Liang, Y., Zhai, Y., Wang, S., Yin, Y., & Lin, J. (2026). Refining microstructure and enhancing mechanical properties of high Nb containing TiAl alloy via multidirectional forging. *Materials Science and Engineering: A, 964*, 150233. https://doi.org/10.1016/j.msea.2026.150233

[14] Taghiabadi, R., & Moharami, A. (2021). Mechanical properties enhancement of Mg–4Si in-situ composites by friction stir processing. *Materials Science and Technology, 37*(1), 66-77.

[15] Naik, M. V., Narasaiah, N., Chakravarthy, P., & Kumar, R. A. (2024). Microstructure and mechanical properties of friction stir processed Zn-Mg biodegradable alloys. *Journal of Alloys and Compounds, 970*, 172160. https://doi.org/10.1016/j.jallcom.2023.172160

[16] Lu, K., Ma, L., Fu, T., Cui, Q., & Ji, S. (2024). Changes in effective grain delineation criteria induced by strong texturing of Zn-0.15Mg alloys after friction stir processing. *Materials Letters, 357,* 135751. https://doi.org/10.1016/j.matlet.2023.135751

[17] Soustani, M. F., Taghiabadi, R., Jafarzadegan, M., & Vasheghani Farahani, M. (2019). Effect of multi-pass friction stir processing on microstructure and mechanical properties of cast Al-7Fe-5Ni alloy. *Materials Research Express, 6*(10), 106571. https://doi.org/10.1088/2053-1591/ab3829

[18] Dong, Z., Han, C., Zhao, Y., Huang, J., Ling, C., Hu, G., Wang, Y., Wang, D., Song, C., & Yang, Y. (2024). Role of heterogenous microstructure and deformation behavior in achieving superior strength-ductility synergy in zinc fabricated via laser powder bed fusion. *International Journal of Extreme Manufacturing*, *6*(4), 045003. https://doi.org/10.1088/2631-7990/ad3929

[19] Vida, T. A., Brito, C., Lima, T. S., Spinelli, J. E., Cheung, N., & Garcia, A. (2019). Near-eutectic Zn-Mg alloys: Interrelations of solidification thermal parameters, microstructure length scale and tensile/corrosion properties. *Current Applied Physics*, *19*(5), 582-598. https://doi.org/10.1016/j.cap.2019.02.013

[20] Lu, Y. U. (2014). *Microstructure and degradation behaviour of Mg-Zn (-Ca) alloys* [Doctoral dissertation, University of Birmingham].

[21] Liu, Z., Qiu, D., Wang, F., Taylor, J. A., & Zhang, M. (2016). Effect of Grain Refinement on Tensile Properties of Cast Zinc Alloys. *Metallurgical and Materials Transactions A*, *47*(2), 830-841. https://doi.org/10.1007/s11661-015-3229-1

[22] Ganjehfard, K., Taghiabadi, R., Noghani, M. T., & Ghoncheh, M. H. (2021). Tensile properties and hot tearing susceptibility of cast Al-Cu alloys containing excess Fe and Si. *International Journal of Minerals, Metallurgy and Materials, 28*(4), 718-728. https://doi.org/10.1007/s12613-020-2039-7

[23] Stolyarov, V. V., Zhu, Y. T., Alexandrov, I. V., Lowe, T. C., & Valiev, R. Z. (2001). Influence of ECAP routes on the microstructure and properties of pure Ti. *Materials Science and Engineering: A*, *299*(1), 59-67. https://doi.org/10.1016/S0921-5093(00)01411-8

[24] Huang, H., Li, G., Jia, Q., Bian, D., Guan, S., Kulyasova, O., Valiev, R. Z., Rau, J. V., & Zheng, Y. (2022). Recent advances on the mechanical behavior of zinc based biodegradable metals focusing on the strain softening phenomenon. *Acta Biomaterialia, 152*, 1-18. https://doi.org/10.1016/j.actbio.2022.08.041

[25] Aghajani, S., & Alizadeh, R. (2024). Severe plastic deformation of Zn and Zn-based alloys. *Journal of Materials Research and Technology*, *33*, 6508-6533. https://doi.org/10.1016/j.jmrt.2024.10.240

[26] Purcek, G., Altan, B. S., Miskioglu, I., & Ooi, P. H. (2004). Processing of eutectic Zn–5% Al alloy by equal-channel angular pressing. *Journal of Materials Processing Technology*, *148*(3), 279-287. https://doi.org/10.1016/j.jmatprotec.2004.02.010

[27] Cao, F., Liu, R., Kong, S., Guo, N., Xu, P., & Xu, G. (2023). Microstructural evolution, high temperature tensile deformation behavior, and deformation mechanism in an Mg–Zn–Y–Ca–Zr alloy processed by multidirectional forging and hot rolling. *Journal of Materials Research and Technology*, *27*, 6729-6743. https://doi.org/10.1016/j.jmrt.2023.11.145

[28] Mollaei, N., Fatemi, S. M., Aboutalebi, M. R., Razavi, S. H., & Bednarczyk, W. (2025). Microstructure, texture, mechanical properties, and corrosion behavior of biodegradable Zn-0.2Mg alloy processed by multi-directional forging. *Acta Metallurgica Sinica (English Letters)*, *38*(3), 507-525. https://doi.org/10.1007/s40195-024-01792-z

[29] Yousefi, D., Taghiabadi, R., & Shaeri, M. H. (2021). Effect of multi-pass multi-directional forging on tribological properties of Si-rich eutectoid ZA alloys. *Transactions of Nonferrous Metals Society of China*, *31*(7), 2024-2038. https://doi.org/10.1016/S1003-6326(21)65635-2

[30] Wang, L., Lou, D., Sun, S., Ren, Y., Qin, G., Bai, P., & Zhao, Z. (2022). Microstructure evolution of Zn–0.2 Mg–0.8 Mn (wt-%) alloys with different initial textures during room-temperature compression. *Materials Science and Technology*, *38*(16), 1368-1375. https://doi.org/10.1080/02670836.2022.2078936

[31] Akbari, F., Taghiabadi, R., Yazdi, M. S., & Ansarian, I. (2024). Tribology characteristics of novel Zn–Si alloys severely deformed by multi-directional forging. *Archives of Civil and Mechanical Engineering*, *24*(4), 225. https://doi.org/10.1007/s43452-024-01033-1

[32] He, L., Cai, J., Wang, Y., Zhang, Y., Xiao, L., Chen, Z., Chen, W., Yu, H., Li, X., Zhang, Q., & Wang, X. (2026). Twin-induced strengthening biodegradable ZnMg alloys for the orthopedic implants. *Biomaterials Advances*, *183*, 214772. https://doi.org/10.1016/j.bioadv.2026.214772

[33] Neres da Silva, N. A., Pereira, P. H. R., Siqueira Corrêa, E. C., Paulino Aguilar, M. T., & Cetlin, P. R. (2021). Microstructural evolution and mechanical properties in a Zn–Al–Cu–Mg hypoeutectic alloy processed by multi-directional forging at room temperature. *Materials Science and Engineering: A, 801*, 140420. https://doi.org/10.1016/j.msea.2020.140420

[34] Liu, Z., Qiu, D., Wang, F., Taylor, J. A., & Zhang, M. (2015). Grain refinement of cast zinc through magnesium inoculation: Characterisation and mechanism. *Materials Characterization*, *106*, 1-10. https://doi.org/10.1016/j.matchar.2015.05.011

[35] Sun, Z., Zhu, X., Li, M., Yang, L., Jiang, J., Zhang, Q., & Song, Z. (2026). Microstructure evolution, mechanical properties, degradation properties, and cytocompatibility of high-strength and high-toughness Zn-0.45Li ultrafine wire. *Journal of Alloys and Compounds*, 1066, 188285. https://doi.org/10.1016/j.jallcom.2026.188285

[36] Rana, K., Razaghian, A., Moharami, A., & Taghiabadi, R. (2026). Achieving synergistic strength-ductility improvement in as-cast Ca-modified Mg–Mg2Si composites through multi-pass FSP and Cu addition.

*Journal of Materials Research and Technology*, *40*, 3007-3024. https://doi.org/10.1016/j.jmrt.2026.01.017

[37] Kishchik, M. S., Mochugovskiy, A. G., Cuda, M., Kishchik, A. A., & Mikhaylovskaya, A. V. (2023). Particle stimulated nucleation effect for Al-Mg-Zr-Sc alloys with Ni addition during multidirectional forging. *Metals*, *13*(8), 1499. https://doi.org/10.3390/met13081499

[38] Yang, P., & Zhao, P. (2023). Void nucleation at dislocation boundaries aided by the synergy of multiple dislocation pile-ups. *International Journal of Plasticity*, *171*, 103779. https://doi.org/10.1016/j.ijplas.2023.103779

[39] Mukherjee, I., & Das, P. (2024). Microstructure evolution during solidification in a low superheat casting process of the Al-Mg2Si composites having excess Si: A phase field study. *Materials Today Communications*, *40,* 109620. https://doi.org/10.1016/j.mtcomm.2024.109620

[40] Wang, Y. Q., Kong, G., Che, C. S., Weng, T. Y., & Sun, Z. W. (2018). Corrosion behavior of Zn-Mg alloys in saturated Ca(OH)2 solution. *Corrosion Science*, *136*, 374-385. https://doi.org/10.1016/j.corsci.2018.03.032

[41] Vida, T. A., Conde, A., Freitas, E. S., Arenas, M. A., Cheung, N., Brito, C., de Damborenea, J., & Garcia, A. (2017). Directionally solidified dilute Zn-Mg alloys: Correlation between microstructure and corrosion properties. *Journal of Alloys and Compounds*, *723*, 536-547. https://doi.org/10.1016/j.jallcom.2017.06.228

[42] Vida, T. A., Freitas, E. S., Cheung, N., Garcia, A., & Osório, W. R. (2017). Electrochemical Corrosion Behavior of as-cast Zn-rich Zn-Mg Alloys in a 0.06M NaCl Solution. *International Journal of Electrochemical Science*, *12*(6), 5264-5283. https://doi.org/10.20964/2017.06.37

[43] Guo, J., He, Z., Zhang, Z., Wang, W., Xu, J., Chen, Z., Liu, T., & Guo, L. (2024). Influence of heat treatment on the microstructure evolution and corrosion performance of biodegradable Zn-Mg alloys. *Materials Today Communications*, *40,* 109976. https://doi.org/10.1016/j.mtcomm.2024.109976

[44] Hesami, L., Taghiabadi, R., Ghoncheh, M. H., Emami, M., & Yazdi, M. S. (2023). Effect of Cu addition on microstructure and corrosion behavior of Al–15Mg2Si composite. *Materials Testing*, *65*(10), 1498-1507. https://doi.org/10.1515/mt-2023-0217

[45] Safary, E., Taghiabadi, R., Ghoncheh, M. H., Emami, M., & Yazdi, M. S. (2024). Effect of solidification cooling rate on corrosion behavior of Al-15Mg2Si composites. *Materials Today Communications*, *38*, 107948. https://doi.org/10.1016/j.mtcomm.2023.107948

[46] Krieg, R., Vimalanandan, A., & Rohwerder, M. (2014). Corrosion of zinc and Zn-Mg alloys with varying microstructures and magnesium contents. *Journal of The Electrochemical Society*, *161*(3), C156. https://doi.org/10.1149/2.103403jes

[47] Ye, L., Huang, H., Sun, C., Zhuo, X., Dong, Q., Liu, H., Ju, J., Xue, F., Bai, J., & Jiang, J. (2022). Effect of grain size and volume fraction of eutectic structure on mechanical properties and corrosion behavior of as-cast Zn–Mg binary alloys. *Journal of Materials Research and Technology*, *16,* 1673-1685. https://doi.org/10.1016/j.jmrt.2021.12.101

[48] Şahbaz, M., & Nalkıran, S. (2026). Microstructural refinement and mechanical property enhancement of AZ91 magnesium alloy via room-temperature multi-directional forging. *Scientific Reports*, *16*(1), 9745. https://doi.org/10.1038/s41598-026-42311-7